

Measurement-induced skin effect and the absence of entanglement phase transition

Jie Ren,^{1,2} Yupeng Wang,^{1,2} and Chen Fang^{1,3,4}

¹*Beijing National Laboratory for Condensed Matter Physics and Institute of Physics, Chinese Academy of Sciences, Beijing 100190, China*

²*University of Chinese Academy of Sciences, Beijing 100049, China*

³*Songshan Lake Materials Laboratory, Dongguan, Guangdong 523808, China*

⁴*Kavli Institute for Theoretical Sciences, Chinese Academy of Sciences, Beijing 100190, China*

Recent developments on the measurement-induced phase transition provide new insight into the dynamical phases of matters. A monitored system undergoes an entanglement transition from (sub)extensive to area law entropy scaling with an increasing measurement rate. Despite the knowledge of this universal behavior observed in both interacting and free systems, we propose that the entanglement transition may break down for (open boundary) systems subjected to some generalized measurement taking the form of projective monitoring with conditional feedback. We show that some generalized measurements, however weak they are, cause the particles to accumulate toward the edge, leading to an anomalous late-time localization phenomenon reminiscent of the “skin effect” in non-Hermitian systems. Such particle localization, named the measurement-induced skin effect, will suppress the entanglement generation and render the system short-range entangled without any entanglement transition. This scheme also provides a route to experimentally implement the skin effect without post-selections.

Introduction.— The competition between the measurement and unitary evolution produces a novel entanglement phase transition [1–9]. In contrast to the generic thermalization dynamics where a closed system eventually evolves to a long-range entangled state with local observables relaxing to their thermal values [10–13], measurements destroy the quantum coherence and render the system short-range entangled. A prototypical model displaying this competition is a random circuits [14–18] interspersed by onsite measurements [1–3]. Numerical simulations reveal an entanglement transition, called the *measurement-induced phase transition* (MIPT), from a volume-law weakly-measured regime to an area-law strongly-measured regime. At the transition point, the system appears to have conformal invariance, implying an underlying (non-unitary) conformal field theory [19–21]. Besides the random circuit systems, later researches find entanglement transitions in the context of monitored fermions [22–27], monitored open systems [28, 29], circuits with pure measurements [30, 31], random tensor network [32–35], and quantum error correction thresholds [36–39].

Quantum measurements introduce intrinsic randomness to the originally deterministic dynamics, with each set of recorded measurement results corresponding to a specific trajectory [40]. Among various frameworks trying to explain the MIPT [23, 27, 36–39, 41–47], one approach boils down to focusing on a specific trajectory, of which the dynamics is described by a non-Hermitian Hamiltonian [48–52]. On the other hand, it is known that non-Hermitian Hamiltonians may induce the so-called *non-Hermitian skin effect* [53–57], which cause an extensive number of particles localizing near the open edges. The skin effect significantly impacts the steady-state entanglement since the accumulation of particles near the boundary and the Pauli exclusive principle forbid a large

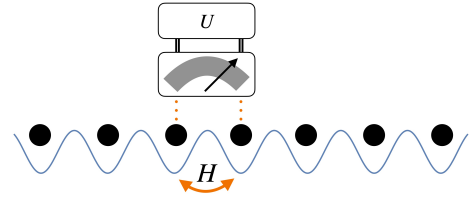


FIG. 1. Schematic of a fermion chain under nearest neighbor interaction and generalized monitoring on each pair of neighboring sites. Unitary feedback will be applied if the probe records a quantum jump.

amount of entanglement. Therefore, the appearance of the skin effect suggests the absence of MIPT. This simple argument, however, relies on the assumption that the particular non-Hermitian evolution is enough to represent the whole ensemble of trajectories, which is generally not true. The non-Hermitian dynamics, nevertheless, can be enforced by post-selection where there are exponentially many experiments carried out, from which the desired measurement record is selected. Due to the experimental difficulty in implementing the post-selected many-body dynamics, a natural question is whether the skin effect can appear without resorting to post-selection.

We address this question assertively, provided that the measurement is in its general form. An axiom in quantum mechanics says that measurement is a complete set of projection operators. Such projective measurement, however, is an idealized approximation because to detect a quantum state, we need a probe that interacts with the system, which will inevitably disturb the measured states. Mathematically, the generalized measurement is formulated as the *positive operator-valued measure* [58, 59]. For a Hamiltonian system, we usually consider the continuous, coarse-grained version of the moni-

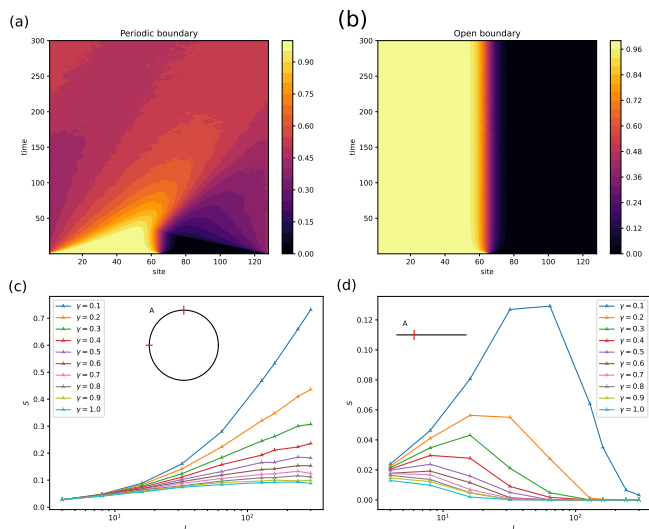


FIG. 2. Simulation of the monitored free fermion model. (a)(b) Trajectory-averaged dynamics of onsite particle density, starting from a half-filled product state $|1 \dots 10 \dots 0\rangle$. The system size is $L = 128$, the measurement rate $\gamma = 0.3$, and the time span $(0, 300)$. (a) Under periodic boundary conditions, the density eventually disperses to a homogeneous distribution, while (b) the steady-state displays strong particle localization under open boundary conditions. (c) Steady-state entanglement entropy $S(L/4)$ under periodic boundary conditions. Entropy scaling shows a transition from sub-extensive logarithmic growth to an area law. (d) Steady-state entanglement entropy $S(L/4)$ under open boundary condition. The entropies approach zero for large enough system sizes, and no entanglement transition happens.

tored dynamics, formulated as the *stochastic Schrödinger equation* (see Appendix A for details), consisting of an effective Hamiltonian and random *quantum jump* processes [60–62]. In this study, we consider the generalized monitorings taking the form of projective quantum jumps followed by conditional unitary operators (as shown in Fig. 1). We note that such measurements with conditional feedback have appeared in the literature as a scheme to construct desired quantum states [63] or dynamics [64].

The central result of this work is the discovery of a measurement-induced skin effect (MISE) in the monitored fermion systems, featuring a particle localization near the edge (under open boundary conditions), as displayed in Fig. 2(b). We demonstrate that for some types of monitoring, MISE appears at an arbitrarily small measurement rate, and thus implies an anomalous boundary sensitivity: under the open boundary condition, the accumulation of particles suppresses the formation of entanglement, leading to an area-law entangled state, while under periodic boundary conditions, regular MIPT persists [see Fig. 2(c)(d)]. We further argue that the MISE survives when the interaction is turned on, which predicts the absence of the universal volume-to-area-law transition for monitored interacting systems. Besides, in con-

trast to the single-body non-Hermitian dynamics from post-selection, MISE provides a many-body version of the skin effect, which appears naturally in the context of the open quantum system.

Skin effect in monitored dynamics.— The evolution of the monitored fermion chain can be described by the stochastic Schrödinger equation [60–62]:

$$d|\psi\rangle = -iH_{\text{eff}}|\psi\rangle dt + \sum_m \left[\frac{L_m}{\langle L_m^\dagger L_m \rangle^{\frac{1}{2}}} - 1 \right] |\psi\rangle dW_m, \quad (1)$$

where the effective non-Hermitian Hamiltonian is

$$H_{\text{eff}} = H - \frac{i\gamma}{2} \sum_m L_m^\dagger L_m, \quad (2)$$

in which H is the system Hamiltonian, L_m the jump operators specifying the observables we monitor, and γ the measurement rate. Each dW_m is an independent Poisson random variable describing the event of random quantum jumps (see Appendix A for detail). Unlike many previous studies, in this work, we consider L_m that acts on two adjacent sites and takes the form

$$L_m = U_m P_m \quad (3)$$

instead of being a projector. The prototypical model we consider involves the measurements described by the projector

$$P_i = \frac{1}{2}(c_i^\dagger - ic_{i+1}^\dagger)(c_i + ic_{i+1}) \quad (4)$$

followed by a conditional unitary operator U_i not yet specified. The effective non-Hermitian Hamiltonian is (note that the choice of U_m does not affect H_{eff})

$$H_{\text{eff}} = \sum_i \left[t_L c_i^\dagger c_{i+1} + t_R c_{i+1}^\dagger c_i - \frac{i\gamma}{4}(n_i + n_{i+1}) \right], \quad (5)$$

where $t_{L/R} = 1 \pm \gamma/4$, is the Hatano-Nelson model [65] displaying non-Hermitian skin effect. For the particular trajectory with no jump recorded, no MIPT will be expected as the result of the skin effect. On the other hand, the (averaged) dynamic of particle density is equivalently described in the density matrix formalism by the Lindblad master equation [66–68]:

$$\frac{d}{dt}\rho = -i[H, \rho] - \frac{\gamma}{2} \sum_m \{L_m^\dagger L_m, \rho\} + \gamma \sum_m L_m \rho L_m^\dagger, \quad (6)$$

where $\rho = \overline{|\psi\rangle\langle\psi|}$ is the trajectory-averaged density matrix. For the projective measurements $L_i = P_i$, the maximally mixed state (within a given particle-number sector) is a nonequilibrium steady state. Moreover, the steady state of Lindblad equation we consider, within a given symmetry sector, is unique [69–72] (see Appendix B for the proof). Therefore, the particle distribution is homogeneous when considering the trajectory averaging, without any particle localization.

Such a no-go principle for skin effect also manifests in the stochastic dynamics picture. The projective measurement P_i measures the occupation of the local quasi-mode $d^\dagger = c_i^\dagger - i c_{i+1}^\dagger$ which is a right-moving wave packet [73]. The effective Hamiltonian H_{eff} describes the dynamics where no such mode is detected, and therefore the left-moving mode is probabilistically favored. In the projective measurement case, the detected right-moving quasimodes will balance out the momentum distribution, leaving a steady state of homogeneity. The balance will be broken by the measurement feedback $U_i \neq \mathbb{I}$, and the steady state can be qualitatively different. Here we consider a simple case where

$$U_i = \exp(i\theta n_{i+1}) \quad (7)$$

is a θ -phase gate acting on site $(i+1)$. Taking the $\theta = \pi$ case for example, the unitary feedback will convert the detected d^\dagger mode to $\tilde{d}^\dagger = c_i^\dagger + i c_{i+1}^\dagger$, a left-moving quasi-mode. The net effect of non-Hermitian and quantum jumps thus leads to a left-moving tendency for all particles, resulting in the MISE.

Free fermion model.— We first consider the free fermion case

$$H = \sum_i (c_i^\dagger c_{i+1} + c_{i+1}^\dagger c_i) \quad (8)$$

and $U_i = e^{i\pi n_{i+1}}$. Note that the corresponding Lindblad equation for operator $L_i = U_i P_i$ is generally non-integrable and thus computationally inaccessible. Nonetheless, by taking the trajectory average of observables, the stochastic evolution (1) provides an efficient numerical method (see Appendix C for details) for the dynamics of averaged observable (or entanglement), as long as U_i preserves the Gaussian state [74].

The steady-state displaying MISE [as shown in Fig. 2(b)] features in two domains where n_i only takes the value of 1 or 0. The “domain wall” in between is the only nontrivial part of the steady state. We characterize the particle localization by the *classical entropy* of particle distribution:

$$S_{\text{cl}} \equiv - \sum_i [\langle n_i \rangle \log \langle n_i \rangle + (1 - \langle n_i \rangle) \log(1 - \langle n_i \rangle)]. \quad (9)$$

This quantity is closely related to MISE since only the nontrivial density (i.e. $\langle n_i \rangle \neq 0, 1$) contributes to S_{cl} . Therefore the asymptotic behavior $S_{\text{cl}} \sim O(1)$ for $L \rightarrow \infty$ implies MISE. In addition, S_{cl} also imposes an upper bound for the entanglement entropy. Note that the entanglement entropy satisfies the *subadditivity* [58, 59]:

$$S_{AB} \leq S_A + S_B. \quad (10)$$

For any bipartite system with subsystems A and B ,

$$S_A + S_B \leq \sum_i S_i \leq S_{\text{cl}}, \quad (11)$$

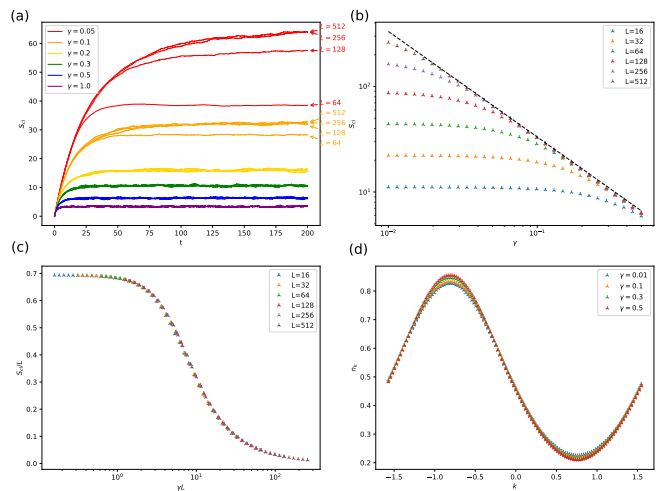


FIG. 3. (a) Time evolution of classical entropy with different measurement rates $\gamma = \{0.05, 0.1, 0.2, 0.3, 0.5, 1.0\}$ and system sizes $L = \{64, 128, 256, 512\}$. The dynamics show no size dependency for $\gamma \geq 2$. (b) Classical entropy of steady states with different measurement rates and system sizes. The data point is plotted in the log-log coordinate. In the thermodynamic limit, data approach the line $\log \gamma + \log S_{\text{cl}} \approx 1.2$. (c) Collapsing of classical entropy to the scaling form in Eq. (13). (d) Steady-state particle distribution in momentum space under periodic boundary conditions for $\gamma = \{0.01, 0.1, 0.3, 0.5\}$.

where the last inequality follows from the fact that the eigenvalues of a positive 2×2 matrix majorize [75] the diagonal elements, and thus have less entropy. Since $S_A = S_B$, the entanglement entropy of any possible bipartition is bounded by half of the classical entropy.

In Fig. 3(a), we simulate the evolution of the classical entropies, starting from a product state with the left half part filled: $|\psi_0\rangle = |1 \cdots 10 \cdots 0\rangle$. Note that for a fixed measurement rate γ and sufficiently large size L , the evolution of S_{cl} becomes independent of L : the sites near the boundary are static, and the sharp edge in the middle blur to a domain wall [see Fig. 2(b)]. The system reaches the steady state with characteristic relaxation time $t^* \sim \gamma^{-1}$, the classical entropy for which, as shown in Fig. 2(b), has the asymptotic behavior

$$S_{\text{cl}}(\gamma, L \rightarrow \infty) = \frac{3.3 \cdots}{\gamma} \quad (12)$$

in the thermodynamic limit. This implies that the characteristic length for the domain wall is $L^* \sim \gamma^{-1}$. Eq. (12) therefore predicts the area-law entanglement scaling $S \leq c/\gamma$ for arbitrary small γ . Moreover, in Fig. 2(c), we observe the density profile has a scale invariance:

$$S_{\text{cl}}(\gamma, L) = Lf(\gamma L), \quad (13)$$

where the scaling function $f(x) \rightarrow 0$ in the $x \rightarrow \infty$ limit. This provides another evidence for MISE in the $\gamma \rightarrow 0$ limit: the scaling behavior (13) implies that even for tiny

γ , when $L \gg \gamma^{-1}$, the density of classical entropy, and thus the entanglement entropy, approach zero.

The skin effect also manifests itself in the periodic boundary condition. By simulating the system with identical parameters but under periodic boundary conditions, we show in Fig. 2(d) that there is an imbalance in the momentum distribution even for the $\gamma \ll 1$ case. We can characterize such imbalance by the current:

$$J[n_k] \equiv \int_{-\pi}^{\pi} dk v_k n_k, \quad (14)$$

where in the $\gamma \ll 1$ limit, we can approximate the velocity by the dispersion of free Hamiltonian:

$$v_k \simeq \partial_k E(k) = \sin(k). \quad (15)$$

For $\gamma = 0.01$ case, $J \approx -0.94$. The nonzero current suggests the skin effect under open boundary condition.

In the above analysis, we consider only the $\theta = \pi$ case in Eq. (7), while similar MISE appears for arbitrary θ . In Appendix D, we show the numerical results for $\theta \neq \pi$. The length of the domain wall, however, is minimized at $\theta = \pi$. When θ approaches zero, we expect that the MISE still appears, although with a large domain wall that may exceed the numerical simulation capability. Therefore, for the projector P_i in Eq. (4), arbitrary measurement feedback can result in an extreme boundary sensitivity due to MISE.

Interacting system.— In the following, we demonstrate that MISE persists in the interacting system. We will focus on the Hamiltonian with nearest neighbor density-density interaction:

$$H = \sum_i (c_i^\dagger c_{i+1} + c_{i+1}^\dagger c_i + g n_i n_{i+1}). \quad (16)$$

The continuous monitoring is the same as the free fermion case. We note that previously, the MIPT for the interacting system is usually on the quantum circuit system with projective measurement. Meanwhile, we show in Fig. 4(a) that systems under continuous monitoring also support a similar entanglement transition (under periodic boundary conditions). Under open boundary conditions, we show in Fig. 4(b) a typical dynamical trajectory, which is qualitatively the same as MISE appearing in monitored free fermion systems.

In the presence of MISE, the only active part of the dynamics is the formation and fluctuation of the domain wall. This enables us to simulate the time evolution for large system sizes using the TEBD algorithm [76, 77] based on the matrix-product states [78, 79]. We calculate the steady-state classical entropy for different γ , with system size L up to 50 [see Fig. 4(c)]. The numerics shows that at least for $\gamma > 0.4$, the classical entropy satisfies the similar scaling law:

$$S_{\text{cl}}(\gamma, L \rightarrow \infty) \propto \gamma^{-1}. \quad (17)$$

This scaling implies the numerical hardness in the small γ regime. Although we are not able to numerically check

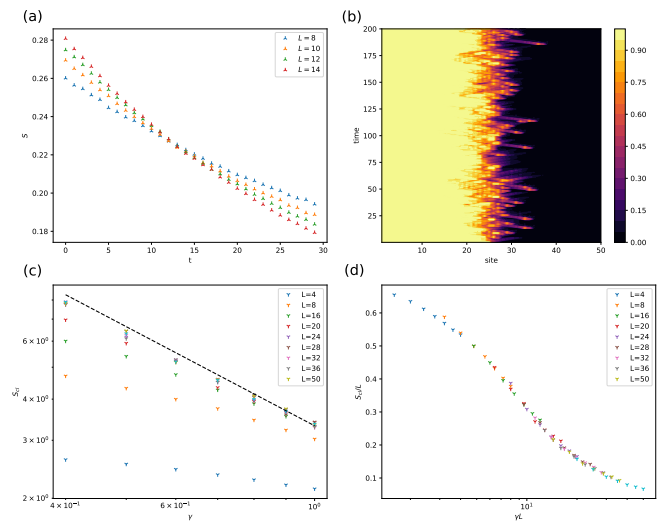


FIG. 4. (a) Steady-state entanglement entropy of monitored interacting (periodic boundary) fermion chain for different γ , where the coupling constant is $g = 1.0$. The data cross at $\gamma \simeq 0.14$ indicates an entanglement transition. (b) A trajectory of a monitored system ($L = 50, \gamma = 0.4$) under open boundary conditions. The active part is at the boundary of two frozen domains. (c) Steady-state classical entropy for monitored fermion chain under open boundary condition. The interacting coupling constant is $g = 1.0$, and the data points are chosen at $\gamma = \{0.4, 0.5, 0.6, 0.7, 0.8, 0.9, 1.0\}$, $L = \{4, 8, 12, 16, 20, 24, 28, 32, 36, 50\}$. The large-size limit of the data is the line $\log \gamma + \log S_{\text{cl}} \approx 1.2$ (d) Data collapsing of classical entropies in the form of Eq. (13).

the scaling behavior in the small γ limit, from the finite size simulation, we obtain the same scaling law as in Eq. (13) [as displayed in Fig. 4(d)]. Therefore, we expect that in the thermodynamics limit, when $L \gg \gamma^{-1}$, the density of the entanglement entropy approaches zero, indicating an area law.

Discussion.— In this work, we consider the effect of imperfect monitoring, formulated as a projective measurement followed by unitary feedback, on the measurement-induced phase transition. The discovery of the measurement-induced skin effect suggests that conditional feedback can qualitatively change the nonequilibrium steady state. Therefore, the entanglement phase structure may be enriched when considering dynamics under generalized measurements. Also, this study shows that MISE may appear in open or (generalized) monitored systems. This provides a route to experimentally implement a many-body skin effect without post-selection.

Note added.— In the middle of this work, we became aware of a recent work [80], which also considers the effect of conditional feedback in the context of MIPT. In Ref. [80], the authors utilize the feedback (called the pre-selection) to map the MIPT to a quantum absorbing state transition, which overcomes the exponential overhead of detecting MIPT experimentally. On the other hand, our

work can be regarded as complementary to the problem: instead of revealing, we show that conditional feedback can also destroy the MIPT.

ACKNOWLEDGMENTS

J.R. thanks Chenguang Liang for the valuable discussions. The numerical simulations based on tensor network use the ITensor package [81].

Appendix A: Stochastic Schrödinger Equation

Microscopically, a measurement process involves a short-time interaction between the system and the probe, which are initially separable:

$$|\psi_{AB}\rangle = e^{-iH_{\text{int}}\Delta t}|\psi_A\rangle \otimes |\psi_B\rangle, \quad (\text{A1})$$

where the wave function of the measured system is denoted as $|\psi_A\rangle$ and the probe $|\psi_B\rangle$. When Δt is much smaller than the time scale of the system, the system can be regarded as static during the measurement. Such measurement is called the *strong measurement*. The probe is thought to be a device that can convert quantum information to the classical one, which takes the form of standard projective measurement. That is, suppose the eigenbasis of the probe is $\{|\phi_n\rangle\}$, the probability of getting a record n is

$$p_n = \langle \phi_n | \rho_B | \phi_n \rangle, \quad \rho_B \equiv \text{Tr}_A |\psi_{AB}\rangle \langle \psi_{AB}|, \quad (\text{A2})$$

and the feedback of the measurement to the system is

$$|\tilde{\psi}_A^{(n)}\rangle = \langle \phi_n | e^{-iH_{\text{int}}\Delta t} |\psi_A\rangle \otimes |\psi_B\rangle \equiv M_n |\psi_A\rangle. \quad (\text{A3})$$

The completeness condition requires

$$\sum_n \langle \tilde{\psi}_A^{(n)} | \tilde{\psi}_A^{(n)} \rangle = 1 \implies \sum_n M_n^\dagger M_n = 1. \quad (\text{A4})$$

This is the general form of the measure. In the language of density operator, a measurement is described by a set of operators $\{M_n\}$. A measurement process may record a result n with probability p_n and change the state to:

$$\rho \rightarrow \frac{M_n \rho M_n^\dagger}{\|M_n \rho M_n^\dagger\|}. \quad (\text{A5})$$

If the measurement result is not known, the averaged density matrix after the measurement is

$$\rho \rightarrow \sum_n M_n \rho M_n^\dagger. \quad (\text{A6})$$

Such a map is called the quantum channel [58].

On the other hand, if the strength of system-probe coupling is comparable with the energy scale of the system, which is the case for an open quantum system, the

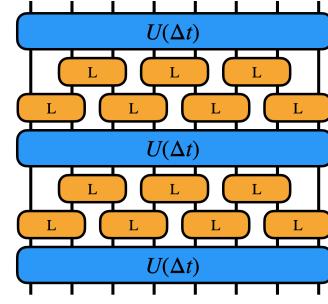


FIG. 5. Circuits representation of the discretized Hamiltonian evolution with constant monitoring.

quantum channel expression should depend on time Δt . Such measurement process is called *weak measurement*. When the system is *Markovian* (the equation of motion depends only on the near past), the course-grained dissipation process can be described by the channel:

$$\begin{aligned} M_n &= L_n \sqrt{\gamma \Delta t}, \\ M_0 &= \left(1 - \sum_{n>0} M_n^\dagger M_n \right)^{1/2} \\ &= 1 - \frac{\gamma}{2} \sum_{n>0} L_n^\dagger L_n \Delta t + O(\Delta t^2). \end{aligned} \quad (\text{A7})$$

For density matrix, the coarse-grained differential equation is the Lindblad equation:

$$\begin{aligned} \frac{d\rho}{dt} &= \lim_{\Delta t \rightarrow 0} \frac{1}{\Delta t} \sum_n M_n e^{-iH\Delta t} \rho e^{iH\Delta t} M_n^\dagger \\ &= -i[H, \rho] - \frac{\gamma}{2} \sum_i \{L_i^\dagger L_i, \rho\} + \gamma \sum_i L_i \rho L_i^\dagger. \end{aligned} \quad (\text{A8})$$

The joint dynamics of Hamiltonian evolution and measurement can be equivalently described by the stochastic process, as shown in Fig. 5, where for each time step Δt , the system first undergoes a coherent evolution $|\psi\rangle \rightarrow e^{-iH\Delta t}|\psi\rangle$, then the application of measurement produces a random process:

$$|\psi\rangle \rightarrow \begin{cases} M_n(\Delta t)|\psi\rangle & P_n = \langle \psi | L_n^\dagger L_n | \psi \rangle \gamma \Delta t \\ M_0(\Delta t)|\psi\rangle & P_0 = 1 - \sum_{n>0} P_n \end{cases}. \quad (\text{A9})$$

Different records of the measurement result correspond to different trajectories, and the Lindblad equation is equivalent to the trajectory averaged of such stochastic processes. In the continuum limit, the stochastic differential equation can be formulated by introducing a Poisson random variable dW_n satisfying the orthogonal condition

$$dW_m dW_n = \delta_{mn} dW_m, \quad (\text{A10})$$

and has the expectation value:

$$\overline{dW_n} = \langle \psi | L_n^\dagger L_n | \psi \rangle \gamma dt. \quad (\text{A11})$$

The quantum jump process $|\psi\rangle \rightarrow M_n|\psi\rangle$ is described by term

$$d|\psi\rangle = \left(\frac{L_n}{\sqrt{\langle L_n^\dagger L_n \rangle}} - 1 \right) |\psi\rangle dW_n, \quad (\text{A12})$$

the process $|\psi\rangle \rightarrow M_0|\psi\rangle$ takes the form:

$$d|\psi\rangle = -\frac{\gamma}{2} \sum_m (L_m^\dagger L_m - \langle L_m^\dagger L_m \rangle) |\psi\rangle dt, \quad (\text{A13})$$

where the $\langle L_m^\dagger L_m \rangle$ is introduced for the normalization purpose. Together with the coherent evolution, we obtain the stochastic Schrödinger equation in the main text:

$$d|\psi\rangle = -iH_{\text{eff}}|\psi\rangle dt + \sum_m \left(\frac{L_m}{\sqrt{\langle L_m^\dagger L_m \rangle}} - 1 \right) |\psi\rangle dW_m. \quad (\text{A14})$$

For numerical simulation of Eq. (A14), we can first discretize the time into small interval Δt . The discrete evolution is then

$$|\psi(t + \Delta t)\rangle = \mathcal{M}_{\Delta t}[e^{-iH_{\text{eff}}\Delta t}|\psi(t)\rangle], \quad (\text{A15})$$

where $\mathcal{M}_{\Delta t}$ represents the quantum jump that randomly happened in time interval Δt :

$$\mathcal{M}_{\Delta t}[|\psi\rangle] \propto \prod_{m \in I} L_m |\psi\rangle. \quad (\text{A16})$$

The set

$$I = \{n | r_n < \gamma \langle L_n^\dagger L_n \rangle \Delta t\} \quad (\text{A17})$$

denotes the jump processes, where $\{r_n \in (0, 1)\}$ is a set of independent random variables (with evenly distributed probability).

Appendix B: Uniqueness of nonequilibrium steady state

In Refs. [69, 70] (see review in Ref. [71] and application in Ref. [72]), it was shown that a Lindblad equation has unique nonequilibrium steady state if and only if the set

$$\{H, L_1, L_1^\dagger, L_2, L_2^\dagger, \dots\} \quad (\text{B1})$$

generates (under multiplication and addition) the complete algebra on the Hilbert space. The general proof assumes no conserved quantity for the Lindblad equation. For the particle number conserving case, as we considered in the main text, we can focus on the Hilbert subspace \mathcal{H}_N spanned by N -particle states. The uniqueness condition then says if $\{H, L_1, L_1^\dagger, L_2, L_2^\dagger, \dots\}$ generates the complete algebra on \mathcal{H}_N , the steady state in \mathcal{H}_N will be unique.

We first prove that the Hamiltonian (under open boundary conditions)

$$H = \sum_i (c_i^\dagger c_{i+1} + c_{i+1}^\dagger c_i) \quad (\text{B2})$$

and the projectors

$$P_i = \frac{1}{2}(c_i^\dagger - ic_{i+1}^\dagger)(c_i + ic_{i+1}) \quad (\text{B3})$$

generate the whole algebra. Note H and P_1, P_2 together generate the following particle number operators:

$$\begin{aligned} n_1 - n_3 &= P_2 - P_1 + i[H, P_1 + P_2], \\ n_1 + n_2 &= \frac{1}{2}(P_1 + P_2 + i[H, n_1 - n_3] + n_1 - n_3), \\ n_2 + n_3 &= (n_1 + n_2) - (n_1 - n_3). \end{aligned} \quad (\text{B4})$$

Then, some straightforward algebra lead to

$$\begin{aligned} c_1^\dagger c_2 - c_2^\dagger c_1 &= i(n_1 + n_2) - iP_1, \\ c_1^\dagger c_2 + c_2^\dagger c_1 &= [c_1^\dagger c_2 - c_2^\dagger c_1, n_2 + n_3], \\ c_2^\dagger c_3 - c_3^\dagger c_2 &= i(n_2 + n_3) - iP_2, \\ c_2^\dagger c_3 + c_3^\dagger c_2 &= [n_1 + n_2, c_2^\dagger c_3 - c_3^\dagger c_2]. \end{aligned} \quad (\text{B5})$$

Upon some addition among Eqs. (B5), we obtain the operator $c_1^\dagger c_2, c_2^\dagger c_3$ and their Hermitian conjugates. The commutations of them further produce $c_1^\dagger c_3$ and its conjugate. Also, note that

$$[c_1^\dagger c_2, c_2^\dagger c_1] = n_1 - n_2. \quad (\text{B6})$$

Together with Eqs. (B4), we generate all fermion bilinear terms $c_i^\dagger c_j$ (including $i = j$ case) on sites $(1, 2, 3)$. To proceed, we subtract the hopping terms between sites $(1, 2)$ from H . The resulting operator is equivalent to a shorter chain starting from site 2. We can then utilize the calculation above to obtain all $c_i^\dagger c_j$ terms on sites $(2, 3, 4)$. We eventually obtain all fermion bilinear terms on the chain by applying the strategy iteratively. Note that fermion bilinear terms $c_i^\dagger c_j$ generate the complete algebra within a fixed particle-number sector since any two product states in the sector can be related by applying several fermion hopping terms.

The proof of the uniqueness of steady state for $\{L_n = U_n P_n\}$ is essentially the same. Note that we can generate all P_i terms by $P_i = L_i^\dagger L_i$. The rest of the proof is the same as above.

Appendix C: Free fermion simulation

The free fermion system can be efficiently represented by the Gaussian state [74]. For a particle number

conserving system, the Gaussian state is a quasimode-occupied state, represented by a matrix B :

$$|B\rangle \equiv \prod_{j=1}^N \sum_i B_{ij} c_i^\dagger |0\rangle = \bigotimes_{j=1}^N |B_j\rangle, \quad (\text{C1})$$

where each column B_j is an occupied quasimode. Note that there is an $\text{SU}(N)$ gauge freedom for the matrix B , i.e.,

$$|B'\rangle = |BU\rangle = |B\rangle, \quad (\text{C2})$$

where U is an arbitrary $\text{SU}(N)$ matrix. Such gauge freedom implies that a Gaussian state is entirely specified by the linear subspace spanned by the quasimodes B_i 's.

The random Schrödinger equation can be Trotterized as Eq. (A15). Using the Baker-Campbell-Hausdor formula $e^A B e^{-A} = e^{\text{ad}_A} B$, the nonunitary evolution is

$$\begin{aligned} e^{-iH_{\text{eff}}\Delta t} |B_t\rangle &= \prod_{j=1}^N \sum_i B_{ij} e^{-iH_{\text{eff}}\Delta t} c_i^\dagger e^{iH_{\text{eff}}\Delta t} |0\rangle \\ &= \prod_{j=1}^N \sum_i B_{ij} e^{-i\Delta t [H_{\text{eff}}, \cdot]} c_i^\dagger |0\rangle \\ &= \prod_{j=1}^N \sum_i \sum_k B_{ij} c_k^\dagger [e^{-iH_{\text{eff}}\Delta t}]_{ki} |0\rangle \\ &= \prod_{j=1}^N \sum_k [e^{-iH_{\text{eff}}\Delta t} B_{ij}]_{kj} c_k^\dagger |0\rangle \\ &= |e^{-iH_{\text{eff}}\Delta t} B_t\rangle. \end{aligned} \quad (\text{C3})$$

That is, the matrix is multiplied by the exponential of the effective non-Hermitian (single-body) Hamiltonian matrix. Note that the resulting matrix is not orthogonal anymore, while the state is still well defined by the linear space spanned by those unorthogonal vectors. In general, for a Gaussian state represented by matrix B , we can obtain a canonical form for the representing matrix using the QR decomposition

$$B = Q \cdot R, \quad (\text{C4})$$

where Q is a unitary matrix and R is upper triangular. Note that Q and B span the same linear space, so the Gaussian state can be expressed as $|Q\rangle$.

The supper operator $\mathcal{M}_{\Delta t}$ in Eq. (A15) corresponds to the Poisson jump process, where for each index i , we randomly decide whether a quantum jump process

$$|B\rangle \rightarrow L_i |B\rangle \quad (\text{C5})$$

happens, with probability

$$p_i = \langle B | L_i^\dagger L_i | B \rangle \gamma \Delta t \quad (\text{C6})$$

The L_m 's we choose in the main text have the form

$$L_m = e^{ih} d^\dagger d, \quad (\text{C7})$$

where

$$d^\dagger = \sum_i a_i c_i^\dagger \quad (\text{C8})$$

is a quasimode, and

$$h = \sum_{ij} h_{ij} c_i^\dagger c_j \quad (\text{C9})$$

is a fermion bilinear. The following shows that the Gaussian form is preserved by such jump operator L_m . First, the probability of the jump process is

$$\langle B | L_m^\dagger L_m | B \rangle = \langle B | d^\dagger d | B \rangle = \|d|B\rangle\|^2. \quad (\text{C10})$$

The action of annihilation operator d on $|B\rangle$ is

$$\begin{aligned} d|B\rangle &= \sum_k a_k^* c_k \prod_j \sum_i c_i^\dagger B_{ij} |0\rangle \\ &= \sum_j \langle a | B_j \rangle \bigotimes_{l \neq j} |B_l\rangle, \end{aligned} \quad (\text{C11})$$

so we can obtain the probability

$$p_m = \sum_j |\langle a | B_j \rangle|^2 \gamma \Delta t. \quad (\text{C12})$$

Besides, we can utilize the gauge freedom to choose the basis such that $\langle a | B'_j \rangle = 0$ for $j > 1$. Such matrix B' always exists since we can always find a column j that $\langle a | B_j \rangle \neq 0$ (otherwise, the probability of the jump is zero). We then move the column to the first and define the column as

$$|B'_j\rangle = |B_j\rangle - \frac{\langle a | B_j \rangle}{\langle a | B_1 \rangle} |B_1\rangle, \quad j > 1. \quad (\text{C13})$$

Note that such column transformation does not alter the linear space B spans, while the orthogonality and the normalization might be affected and should be renormalized afterward. Eq. (C11) then simplified to:

$$d|B\rangle = \bigotimes_{j>1} |B'_j\rangle. \quad (\text{C14})$$

The result of the quantum jump is

$$L_m |B\rangle = |e^{ih} a\rangle \bigotimes_{j>1} |e^{ih} B'_j\rangle. \quad (\text{C15})$$

Appendix D: Monitored free fermion with different conditional feedback

In this appendix, we provide more numerical results on the monitored free fermion system with Hamiltonian

$$H = \sum_i (c_i^\dagger c_{i+1} + c_{i+1}^\dagger c_i) \quad (\text{D1})$$

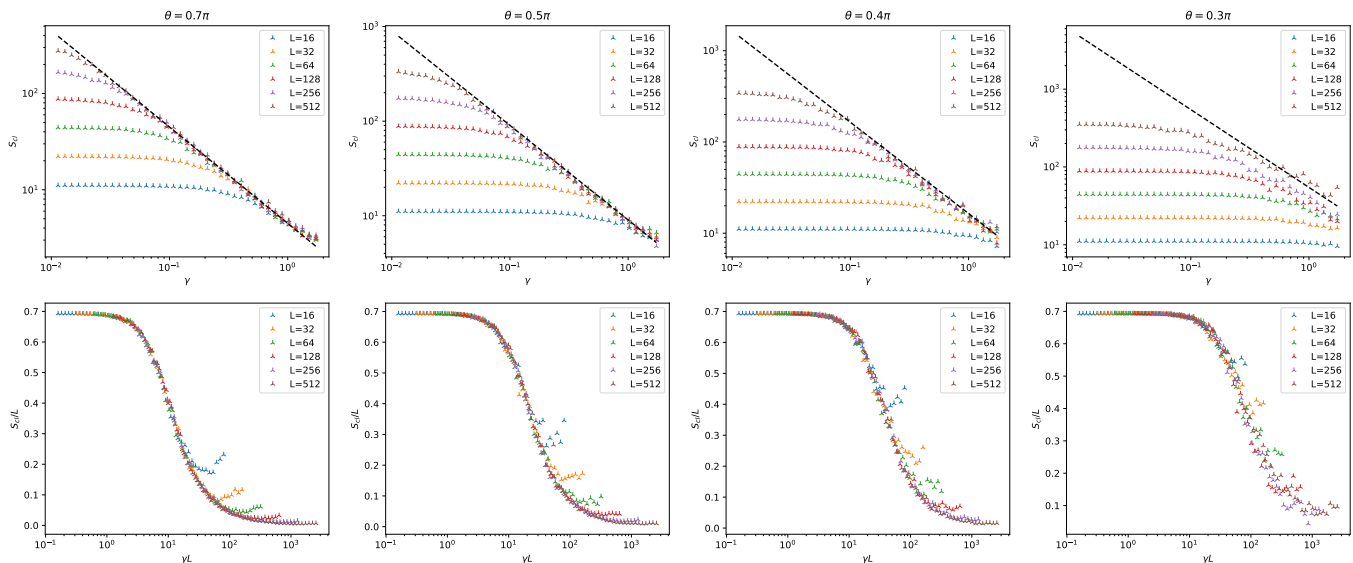


FIG. 6. Steady-state classical entropy for $\gamma = \{0.7\pi, 0.5\pi, 0.4\pi, 0.3\pi\}$. The first line of figures shows the asymptotic behavior. The second line of figures shows the data collapsing. Those outliers are from measurement rate $\gamma \geq 1$.

and the generalized monitoring described by the operator

$$L_i = \frac{1}{2} e^{i\theta n_{i+1}} (c_i^\dagger - i c_{i+1}^\dagger) (c_i + i c_{i+1}). \quad (\text{D2})$$

In Fig. 6, we present the numerical simulation of the monitored system with different θ 's. The steady-state classical entropy all agrees with the general scaling be-

havior: $S_{\text{cl}}(\gamma, L \rightarrow \infty) = c(\theta)/\gamma$. The constants $c(\theta)$ increases as θ decreases:

$$\begin{aligned} c(\pi) &\approx 3.3, & c(0.7\pi) &\approx 4.5, & c(0.5\pi) &\approx 9.0, \\ c(0.4\pi) &\approx 16, & c(0.3\pi) &\approx 55. \end{aligned} \quad (\text{D3})$$

Also, we see that for $\gamma < 1$, the data satisfies the scaling law $S_{\text{cl}} = L f_\theta(\gamma L)$. We thus expect the skin effect to appear for arbitrary θ .

-
- [1] Y. Li, X. Chen, and M. P. A. Fisher, Quantum zeno effect and the many-body entanglement transition, *Phys. Rev. B* **98**, 205136 (2018).
- [2] B. Skinner, J. Ruhman, and A. Nahum, Measurement-induced phase transitions in the dynamics of entanglement, *Phys. Rev. X* **9**, 031009 (2019).
- [3] A. Chan, R. M. Nandkishore, M. Pretko, and G. Smith, Unitary-projective entanglement dynamics, *Phys. Rev. B* **99**, 224307 (2019).
- [4] Y. Li, X. Chen, and M. P. A. Fisher, Measurement-driven entanglement transition in hybrid quantum circuits, *Phys. Rev. B* **100**, 134306 (2019).
- [5] A. Zabalo, M. J. Gullans, J. H. Wilson, S. Gopalakrishnan, D. A. Huse, and J. H. Pixley, Critical properties of the measurement-induced transition in random quantum circuits, *Phys. Rev. B* **101**, 060301 (2020).
- [6] L. Fidkowski, J. Haah, and M. B. Hastings, How Dynamical Quantum Memories Forget, *Quantum* **5**, 382 (2021).
- [7] A. Nahum, S. Roy, B. Skinner, and J. Ruhman, Measurement and entanglement phase transitions in all-to-all quantum circuits, on quantum trees, and in landauinsburg theory, *PRX Quantum* **2**, 010352 (2021).
- [8] M. Ippoliti, M. J. Gullans, S. Gopalakrishnan, D. A. Huse, and V. Khemani, Entanglement phase transitions in measurement-only dynamics, *Phys. Rev. X* **11**, 011030 (2021).
- [9] M. P. A. Fisher, V. Khemani, A. Nahum, and S. Vijay, *Random quantum circuits* (2022).
- [10] J. M. Deutsch, Quantum statistical mechanics in a closed system, *Phys. Rev. A* **43**, 2046 (1991).
- [11] J. M. Deutsch, Eigenstate thermalization hypothesis, *Reports on Progress in Physics* **81**, 082001 (2018).
- [12] M. Srednicki, Chaos and quantum thermalization, *Phys. Rev. E* **50**, 888 (1994).
- [13] L. D'Alessio, Y. Kafri, A. Polkovnikov, and M. Rigol, From quantum chaos and eigenstate thermalization to statistical mechanics and thermodynamics, *Advances in Physics* **65**, 239 (2016), <https://doi.org/10.1080/00018732.2016.1198134>.
- [14] A. Chan, A. De Luca, and J. T. Chalker, Solution of a minimal model for many-body quantum chaos, *Phys. Rev. X* **8**, 041019 (2018).
- [15] A. Nahum, S. Vijay, and J. Haah, Operator spreading in random unitary circuits, *Phys. Rev. X* **8**, 021014 (2018).
- [16] C. W. von Keyserlingk, T. Rakovszky, F. Pollmann, and S. L. Sondhi, Operator hydrodynamics, otocs, and entanglement growth in systems without conservation laws, *Phys. Rev. X* **8**, 021013 (2018).

- [17] T. Zhou and A. Nahum, Emergent statistical mechanics of entanglement in random unitary circuits, *Phys. Rev. B* **99**, 174205 (2019).
- [18] M. P. A. Fisher, V. Khemani, A. Nahum, and S. Vijay, *Random quantum circuits* (2022).
- [19] Y. Li, X. Chen, A. W. W. Ludwig, and M. P. A. Fisher, Conformal invariance and quantum nonlocality in critical hybrid circuits, *Phys. Rev. B* **104**, 104305 (2021).
- [20] X. Chen, Y. Li, M. P. A. Fisher, and A. Lucas, Emergent conformal symmetry in nonunitary random dynamics of free fermions, *Phys. Rev. Research* **2**, 033017 (2020).
- [21] A. Zabalo, M. J. Gullans, J. H. Wilson, S. Gopalakrishnan, D. A. Huse, and J. H. Pixley, Critical properties of the measurement-induced transition in random quantum circuits, *Phys. Rev. B* **101**, 060301 (2020).
- [22] O. Alberton, M. Buchhold, and S. Diehl, Entanglement transition in a monitored free-fermion chain: From extended criticality to area law, *Phys. Rev. Lett.* **126**, 170602 (2021).
- [23] X. Cao, A. Tilloy, and A. D. Luca, Entanglement in a fermion chain under continuous monitoring, *SciPost Phys.* **7**, 024 (2019).
- [24] M. Coppola, E. Tirrito, D. Karevski, and M. Collura, Growth of entanglement entropy under local projective measurements, *Phys. Rev. B* **105**, 094303 (2022).
- [25] T. Müller, S. Diehl, and M. Buchhold, Measurement-induced dark state phase transitions in long-ranged fermion systems, *Phys. Rev. Lett.* **128**, 010605 (2022).
- [26] T. Minato, K. Sugimoto, T. Kuwahara, and K. Saito, Fate of measurement-induced phase transition in long-range interactions, *Phys. Rev. Lett.* **128**, 010603 (2022).
- [27] M. Buchhold, Y. Minoguchi, A. Altland, and S. Diehl, Effective theory for the measurement-induced phase transition of dirac fermions, *Phys. Rev. X* **11**, 041004 (2021).
- [28] B. Ladewig, S. Diehl, and M. Buchhold, Monitored open fermion dynamics: Exploring the interplay of measurement, decoherence, and free hamiltonian evolution, *Phys. Rev. Research* **4**, 033001 (2022).
- [29] X. Turkeshi, L. Piroli, and M. Schiró, Enhanced entanglement negativity in boundary-driven monitored fermionic chains, *Phys. Rev. B* **106**, 024304 (2022).
- [30] A. Lavasani, Y. Alavirad, and M. Barkeshli, Measurement-induced topological entanglement transitions in symmetric random quantum circuits, *Nature Physics* **17**, 342 (2021).
- [31] M. Ippoliti, M. J. Gullans, S. Gopalakrishnan, D. A. Huse, and V. Khemani, Entanglement phase transitions in measurement-only dynamics, *Phys. Rev. X* **11**, 011030 (2021).
- [32] R. Vasseur, A. C. Potter, Y.-Z. You, and A. W. W. Ludwig, Entanglement transitions from holographic random tensor networks, *Phys. Rev. B* **100**, 134203 (2019).
- [33] J. Lopez-Piqueres, B. Ware, and R. Vasseur, Mean-field entanglement transitions in random tree tensor networks, *Phys. Rev. B* **102**, 064202 (2020).
- [34] C.-M. Jian, B. Bauer, A. Keselman, and A. W. W. Ludwig, *Criticality and entanglement in non-unitary quantum circuits and tensor networks of non-interacting fermions* (2020).
- [35] Z.-C. Yang, Y. Li, M. P. A. Fisher, and X. Chen, Entanglement phase transitions in random stabilizer tensor networks, *Phys. Rev. B* **105**, 104306 (2022).
- [36] S. Choi, Y. Bao, X.-L. Qi, and E. Altman, Quantum error correction in scrambling dynamics and measurement-induced phase transition, *Phys. Rev. Lett.* **125**, 030505 (2020).
- [37] M. J. Gullans and D. A. Huse, Scalable probes of measurement-induced criticality, *Phys. Rev. Lett.* **125**, 070606 (2020).
- [38] M. J. Gullans and D. A. Huse, Dynamical purification phase transition induced by quantum measurements, *Phys. Rev. X* **10**, 041020 (2020).
- [39] M. J. Gullans, S. Krastanov, D. A. Huse, L. Jiang, and S. T. Flammia, Quantum coding with low-depth random circuits, *Phys. Rev. X* **11**, 031066 (2021).
- [40] A. J. Daley, Quantum trajectories and open many-body quantum systems, *Advances in Physics* **63**, 77 (2014), <https://doi.org/10.1080/00018732.2014.933502>.
- [41] Y. Bao, S. Choi, and E. Altman, Theory of the phase transition in random unitary circuits with measurements, *Phys. Rev. B* **101**, 104301 (2020).
- [42] C.-M. Jian, Y.-Z. You, R. Vasseur, and A. W. W. Ludwig, Measurement-induced criticality in random quantum circuits, *Phys. Rev. B* **101**, 104302 (2020).
- [43] Y. Li and M. P. A. Fisher, Statistical mechanics of quantum error correcting codes, *Phys. Rev. B* **103**, 104306 (2021).
- [44] Y. Li, R. Vasseur, M. P. A. Fisher, and A. W. W. Ludwig, *Statistical mechanics model for clifford random tensor networks and monitored quantum circuits* (2021).
- [45] X. Turkeshi, M. Dalmonte, R. Fazio, and M. Schiró, Entanglement transitions from stochastic resetting of non-hermitian quasiparticles, *Phys. Rev. B* **105**, L241114 (2022).
- [46] M. Ippoliti and V. Khemani, Postselection-free entanglement dynamics via spacetime duality, *Phys. Rev. Lett.* **126**, 060501 (2021).
- [47] M. Ippoliti, T. Rakovszky, and V. Khemani, Fractal, logarithmic, and volume-law entangled nonthermal steady states via spacetime duality, *Phys. Rev. X* **12**, 011045 (2022).
- [48] G. Kells, D. Meidan, and A. Romito, *Topological transitions with continuously monitored free fermions* (2021).
- [49] X. Turkeshi and M. Schiró, *Entanglement and correlation spreading in non-hermitian spin chains* (2022).
- [50] S.-K. Jian, Z.-C. Yang, Z. Bi, and X. Chen, Yang-lee edge singularity triggered entanglement transition, *Phys. Rev. B* **104**, L161107 (2021).
- [51] K. Kawabata, T. Numasawa, and S. Ryu, *Entanglement phase transition induced by the non-hermitian skin effect* (2022).
- [52] S. Gopalakrishnan and M. J. Gullans, Entanglement and purification transitions in non-hermitian quantum mechanics, *Phys. Rev. Lett.* **126**, 170503 (2021).
- [53] S. Yao and Z. Wang, Edge states and topological invariants of non-hermitian systems, *Phys. Rev. Lett.* **121**, 086803 (2018).
- [54] K. Zhang, Z. Yang, and C. Fang, Correspondence between winding numbers and skin modes in non-hermitian systems, *Phys. Rev. Lett.* **125**, 126402 (2020).
- [55] K. Yokomizo and S. Murakami, Non-bloch band theory of non-hermitian systems, *Phys. Rev. Lett.* **123**, 066404 (2019).
- [56] N. Okuma, K. Kawabata, K. Shiozaki, and M. Sato, Topological origin of non-hermitian skin effects, *Phys. Rev. Lett.* **124**, 086801 (2020).
- [57] Z. Yang, K. Zhang, C. Fang, and J. Hu, Non-hermitian bulk-boundary correspondence and auxiliary generalized

- brillouin zone theory, *Phys. Rev. Lett.* **125**, 226402 (2020).
- [58] M. A. Nielsen and I. L. Chuang, *Quantum Computation and Quantum Information: 10th Anniversary Edition* (Cambridge University Press, 2010).
- [59] M. M. Wilde, *Quantum Information Theory* (Cambridge University Press, 2013).
- [60] K. Jacobs and D. A. Steck, A straightforward introduction to continuous quantum measurement, *Contemporary Physics* **47**, 279 (2006), <https://doi.org/10.1080/00107510601101934>.
- [61] H. M. Wiseman and G. J. Milburn, *Quantum Measurement and Control* (Cambridge University Press, 2009).
- [62] A. Barchielli and M. Gregoratti, The stochastic schrödinger equation, in *Quantum Trajectories and Measurements in Continuous Time: The Diffusive Case* (Springer Berlin Heidelberg, Berlin, Heidelberg, 2009) pp. 11–49.
- [63] T.-C. Lu, L. A. Lessa, I. H. Kim, and T. H. Hsieh, *Measurement as a shortcut to long-range entangled quantum matter* (2022).
- [64] T. Iadecola, S. Ganeshan, J. H. Pixley, and J. H. Wilson, *Dynamical entanglement transition in the probabilistic control of chaos* (2022).
- [65] N. Hatano and D. R. Nelson, Localization transitions in non-hermitian quantum mechanics, *Phys. Rev. Lett.* **77**, 570 (1996).
- [66] G. Lindblad, On the generators of quantum dynamical semigroups, *Communications in Mathematical Physics* **48**, 119 (1976).
- [67] E. B. Davies, Markovian master equations, *Communications in Mathematical Physics* **39**, 91 (1974).
- [68] H.-P. Breuer and F. Petruccione, *The Theory of Open Quantum Systems* (Oxford University Press, 2007).
- [69] D. E. Evans, Irreducible quantum dynamical semigroups, *Communications in Mathematical Physics* **54**, 293 (1977).
- [70] A. Frigerio, Stationary states of quantum dynamical semigroups, *Communications in Mathematical Physics* **63**, 269 (1978).
- [71] H. Spohn, Kinetic equations from hamiltonian dynamics: Markovian limits, *Rev. Mod. Phys.* **52**, 569 (1980).
- [72] T. Prosen, Matrix product solutions of boundary driven quantum chains, *Journal of Physics A: Mathematical and Theoretical* **48**, 373001 (2015).
- [73] Let $d^\dagger = c_i^\dagger - ic_{i+1}^\dagger$, in the momentum space, $d^\dagger = \sum_k f(k)c_k^\dagger$, where the weight $|f(k)|^2 = (1 + \sin k)/2$.
- [74] S. Bravyi, Lagrangian representation for fermionic linear optics [10.48550/ARXIV.QUANT-PH/0404180](https://arxiv.org/abs/10.48550/ARXIV.QUANT-PH/0404180) (2004).
- [75] R. A. Horn and C. R. Johnson, *Topics in Matrix Analysis* (Cambridge University Press, 1991).
- [76] G. Vidal, Efficient classical simulation of slightly entangled quantum computations, *Phys. Rev. Lett.* **91**, 147902 (2003).
- [77] G. Vidal, Classical simulation of infinite-size quantum lattice systems in one spatial dimension, *Phys. Rev. Lett.* **98**, 070201 (2007).
- [78] M. Fannes, B. Nachtergaele, and R. F. Werner, Finitely correlated states on quantum spin chains, *Communications in Mathematical Physics* **144**, 443 (1992).
- [79] M. W. J. C. D. Perez-Garcia, F. Verstraete, Matrix product state representations (2007), [arXiv:quant-ph/0608197](https://arxiv.org/abs/quant-ph/0608197).
- [80] M. Buchhold, T. Müller, and S. Diehl, *Revealing measurement-induced phase transitions by pre-selection* (2022).
- [81] M. Fishman, S. R. White, and E. M. Stoudenmire, The ITensor software library for tensor network calculations (2020), [arXiv:2007.14822](https://arxiv.org/abs/2007.14822).